Analysis of actin filament network organization in lamellipodia by comparing experimental and simulated images

Sébastien Schaub*, Jean-Jacques Meister and Alexander B. Verkhovsky

Laboratory of Cell Biophysics, Ecole Polytechnique Fédérale, Lausanne, Switzerland

*Author for correspondence at present address: UMR 144, Institut Curie, Paris, France (e-mail: sebastien.schaub@curie.fr)

Accepted 12 December 2006
Journal of Cell Science 120, 1491-1500 Published by The Company of Biologists 2007
doi:10.1242/jcs.03379

Summary

Protrusion of lamellipodia during cell migration depends on the assembly of actin network. The assembly mechanism, based on dendritic filament branching, has been investigated in reconstituted in vitro systems, but little is known about the dynamical and structural properties of the actin network in the lamellipodia of migrating cells. The length and orientation of filaments are difficult to measure directly in either optical or electron microscopy images because of the high filament density and overlapping of individual filaments. Here, we use the non-uniformity of optical images of the lamellipodia to extract information about the structural and dynamical properties of the underlying actin network. To determine the relationship between the image features and the properties of the network, we performed simulations of actin network assembly, based on the hypothesis of stochastic branching and capping of filaments, and produced computed 'fluorescence' and 'electron microscopy' images of the simulated network. By varying simulation parameters, in particular the actin filament density, length and orientation, we closely reproduced the contrast and the characteristic diagonal criss-cross pattern observed in the experimental optical images. Thus, matching the images of the simulated network to the experimental images allowed us to estimate parameters of actin filament network in lamellipodia.

Supplementary material available online at
http://jcs.biologists.org/cgi/content/full/120/8/1491/DC1

Key words: Actin, Cytoskeleton, Image processing, Cell movement, Lamellipodia, Modeling

Introduction

Actin polymerization is believed to drive protrusion at the leading edge of migrating cells. One of the major protrusive organelles of the cell is the lamellipodium, a flat, wide and thin pseudopodium filled with a dense actin network. Biochemical and ultrastructural studies have identified the major components and reactions contributing to the assembly of the actin network, but there is a gap between the knowledge at the molecular level and the understanding of how the structure and dynamics of the lamellipodium are defined at the cellular scale.

Dendritic nucleation of filaments mediated by Arp2/3 complex is believed to be a major mechanism of assembly of the lamellipodial actin network (Carlier et al., 2003; Pollard and Borisy, 2003). In vitro studies, using reconstituted model systems, established that only a limited number of proteins are sufficient to sustain directional assembly and generate protrusive force (Carlier et al., 2003; Marcy et al., 2004). New filaments are nucleated as branches at the sides or ends of pre-existing filaments in a process dependent on the Arp2/3 complex (Mullins et al., 1998; Svitkina and Borisy, 1999). The preferential branching angle has been estimated to be 70° (Mullins et al., 1998; Svitkina et al., 1997). A filament elongates until a capping protein binds to the barbed-end and blocks assembly. Subsequent disassembly of filaments is accelerated by ADF/cofilin and serves to replenish the pool of free subunits for continuous assembly. Given this sequence of reactions, the capping rate sets the limit for the length of actin filaments in the lamellipodium, whereas the number of growing filaments is defined by the balance between branching and capping rates. A high capping rate is expected to correlate with a high branching rate because the cell needs to produce more new filament tips to compensate for the loss of the filaments due to capping. Thus, the length of actin filaments in the lamellipodia reflects network dynamics: short filaments might indicate high rates of both capping and branching reactions, whereas long filaments suggest persistent filament growth as well as low rates of capping and branching. In the extreme case, long filaments may reflect a recently suggested alternative, an Arp2/3-independent protrusion mechanism (Gupton et al., 2005). Thus, filament length is diagnostic to elucidate actin network dynamics. Filament length is also important for the mechanical force balance in the protruding lamellipodium. It has been suggested that short filaments are more efficient at pushing the plasma membrane forward in Brownian ratchet mechanism (Mogilner and Oster, 1996; Peskin et al., 1993) because bending rigidity of the filament decreases with its length. Experimentally, the variation of filament length was shown to affect the overall dynamics and stability of the lamellipodium (Bear et al., 1998). However, the exact values of branching and capping rates, and the filament length distribution in the lamellipodium are not known. Electron microscopy (EM) images, obtained using a platinum

replica technique, tend to display frequently branching short filaments (Bear et al., 2002; Svitkina and Borisy, 1999), whereas negatively stained images give the impression of long unbranched filaments (Small, 1995; Small et al., 1995). The lamellipodial actin network is very dense, precluding in most cases the possibility to trace individual filaments in EM images from one end to the other and, therefore, estimations of filament length are subjective. They vary between few hundred nanometers (Bear et al., 2002; Cano et al., 1991) and few micrometers (Small et al., 1995; Xu et al., 1999) depending on the EM approach. It has been argued that individual EM approaches are prone to various artifacts, e.g. some apparent branches may result from the crucial point-drying procedure (Resch et al., 2002).

Orientation of the filaments is another important structural parameter of the lamellipodial network. Actin filaments are generally oriented with their fast-growing barbed-end (Pollard et al., 2000) towards the leading edge (Small et al., 1995). EM images also displayed apparent preferential orientation of filaments along two roughly diagonal lines with respect to the leading edge (Small et al., 1995). Theoretical modeling suggests that this orientation is the most efficient for protrusion (Mogilner and Oster, 1996) and, at the same time, favorable for filament proliferation through the branching process (Maly and Borisy, 2001). Two studies (Maly and Borisy, 2001; Verkhovsky et al., 2003) employed image analysis based on Radon transform to evaluate filament orientation in platinum replica images. The results were consistent with the predicted filament orientation but the outcome depended on the edge-detection procedure (Verkhovsky et al., 2003) and the analyzed population of the filaments exposed on the surface was representative of the whole filament population, which was a matter of concern. Thus, quantitative analysis of the EM images of the actin network presents significant problems due to high filament density and non-uniform visualization of the individual filaments.

However, the potential of optical microscopy to analyze the organization of actin network remains largely unexplored. Although optical fluorescent microscopy has a lower resolution limit compared with EM, it has the advantage to be more amenable to quantitative analysis because the image intensity is directly proportional to the density of actin filaments labeled with fluorescent dye. Optical images of lamellipodia are not uniform but display a characteristic diagonal criss-cross pattern of linear features that is expected to reflect structural properties of the network. Correlative light microscopy and EM analysis showed that the diagonal features observed using light microscopy are due to variation of filament density and that individual filaments are preferentially oriented parallel to these diagonal lines (Verkhovsky et al., 2003). However, it is still unclear how the pattern observed by light microscopy is related to the structural parameters of the network and the growth dynamics of individual filaments. One possibility is that the features observed by light microscopy are related to the intrinsic properties of the mechanism of branching assembly. Another possibility is that they arise because filament grouping is promoted by actin-bundling proteins or other regulatory factors, e.g. as in precursors of the filopodia (Svitkina et al., 2003).

Here, we aimed to establish the relationship between the dynamical and structural parameters of the actin network and the lamellipodium patterns observed in light microscopy and EM images. We simulated images of actin network based on a simple stochastic model of network growth and compared those simulated images to experimental images of lamellipodia of fish epidermal keratocytes. Keratocytes were used as a model system because their wide and flat lamellipodia have a steady-state character of protrusion. Comparison of experimental keratocyte lamellipodia images with simulated images allowed to determine the parameters governing the network structure and dynamics, such as filament length, density and angular distribution.

Results

Our simulations resulted in data sets containing the features of each filament. From these data, we created images (see Materials and Methods) similar to fluorescence and EM (platinum replica and negative staining) images to study the effects of various simulation parameters on the image pattern and compare to the experimental images.

Analysis of image contrast and actin polymer concentration

The variation of actin filament density in keratocyte lamellipodia produced a criss-cross pattern of bright and dark features in the experimental fluorescence images. The relationship between the observed criss-cross pattern and the underlying structure is unknown. We assumed that the fluorescence intensity of phalloidin-stained images is proportional to the density of actin filaments and, thus, a variation of intensity reflects a variation in actin density. We further proposed that variation in filament density resulted from the probabilistic nature of branching and capping reactions. Here, we investigate the parameters controlling the magnitude of variation in filament density and whether the variation in simulated images can be compared to the experimental one.

To measure the variation of intensity in both experimental and simulated images we used the ratio of standard deviation (s.d.) of intensity to the mean intensity of the image. We refer to this ratio as the contrast of the image. For a random distribution, the standard deviation is proportional to the square root of the number of elements. A similar relationship was expected for the simulated images of the lamellipodia, where the variation of filament density arises at the leading edge because of the stochastic fluctuation of branching and capping reactions. Given that the mean image intensity and the standard deviation are, respectively, proportional to the filament concentration and to the square root of it, the contrast is expected to be proportional to the inverse of the square root of the concentration:

$$C = \frac{\text{s.d. } (I)}{I} = \beta \frac{1}{\sqrt{[A]}}, \qquad (1)$$

where C is the contrast, I, the fluorescence intensity, $[A]$, concentration of actin filaments, and β, the proportionality factor. We used τ=250 nm as an estimate of the lamellipodia thickness (Anderson et al., 1996), to convert the simulated two-dimensional amount of actin into a three-dimensional volume of actin. For a distribution of independent random values it is expected that β=1. However, diffraction in the optical microscope results in the intensity values of adjacent pixels being correlated to each other. To estimate the effect of

Fig. 1. Formation of simulated fluorescence image. (a) Diagram of the actin network illustrating filament elongation, branching and capping reactions. (b,c) Simulation, converted into an actin-polymer density map (b) and resolution was reduced to obtain an image similar to the fluorescence image (c).

diffraction on β, diffraction may be equivalent to an increase in the size of the image by a factor that equals the number of pixels in the diffraction spot, without changing image resolution. Then, the contrast of the image would be reduced by the same factor. Assuming the area of the diffraction spot is a circle with the resolution limit as diameter, we obtain:

$$\beta \cong 4 / (\pi \cdot res^2) \cong 0.15 \ . \qquad (2)$$

The analysis of the contrast of simulated images, depending on the concentration, confirmed the above relationship between contrast and concentration. A fit of the simulated data provided an estimate of β=0.18 (Fig. 2b), which is close to the above analytical estimation. Variation of either mean filament length $\Delta\tau$ or R_0 had no effect on the value of β (data not shown); as expected, β depended only on the diffraction spot size (data not shown). Since we used the experimental diffraction-spot size in the simulations, the value of β extracted from the simulations was used to estimate the contribution of random fluctuations of branching and capping to the contrast of the experimental images at any given actin concentration. Actin concentration in the lamellipodium has previously been estimated to be 1580±620 $\mu m/\mu m^3$ = 1200±440 μM (Abraham et al., 1999). Based on the assumption that all contrast of the experimental images results from random factors, we determined the actin concentration in the experimental lamellipodia at approximately 1160±550 $\mu m/\mu m^3$ = 900±400 μM (Fig. 2b, grey zone) which is similar to the above independent estimation (Abraham et al., 1999). Consequently, contrast of the experimental images was fully accounted for by random fluctuations of branching and capping, thus supporting our model of the formation of the optical pattern in the lamellipodial actin network.

Given that the contrast in the lamellipodia results from stochastic processes, contrast measurements were used to determine the absolute concentration of actin filaments throughout the lamellipodium. Note that measurement of the fluorescent intensity provides only a relative measure of actin concentration because the scale factor between the concentration and the intensity is unknown.

Analysis of the variation of polymer density and image contrast with the distance from the leading edge: implications for actin disassembly kinetics

We then analyzed the relationship between actin density and contrast of the image as a function of the distance from the leading edge of the lamellipodium. Based on fluorescence intensity, actin concentration in the lamellipodium decreases gradually from ~0.5 μm behind the leading edge to the back of the lamellipodium (Small et al., 1995; Svitkina et al., 1997) (Fig. 2a, right panel). We measured the mean and standard deviation of the fluorescence intensity for each line parallel to the leading edge in 107 regions of lamellipodia of 22 cells. Measurements of relative actin concentration (based on fluorescence intensity) and of absolute actin concentration (based on contrast) were plotted against the distance from the leading edge that was scaled to the unitary lamellipodium length (Fig. 2d,e). Both methods of measuring actin concentration showed a linear decay from the proximity of the leading edge (x=0) to the back of the lamellipodium (x=1). The mean concentration ratios between front and back of the lamellipodia were 1.73 based on contrast (Fig. 2d) and 1.6, based on intensity (Fig. 2c), which was consistent with previous intensity measurements (Small et al., 1995; Svitkina and Borisy, 1999). The similarity of the two values confirms the accuracy of measurements based on contrast and reinforces the hypothesis of the stochastic nature of the network-assembly process.

The decrease in actin concentration from the front to the back of the lamellipodium is due to depolymerization, which could have an effect on the relationship between contrast and concentration. To evaluate this effect, we added the process of depolymerization to the simulation. We assumed that the entire filament depolymerizes in a single event, provided that the actin is capped and its barbed-end located further than 1 μm away from the leading edge (Svitkina et al., 1997). We considered two types of depolymerization kinetics: first and zero order processes (see Materials and Methods). We adjusted the parameter of the depolymerization rate in the simulation such that the ratio of the fluorescence intensity at the front of the region of interest (higher intensity) to that at the back (lower intensity) was ~1.6. To compare simulated and experimental images, we scaled each region of interest to a unitary length, and plotted the actin density profiles based on either fluorescent intensity or contrast measurements on a distance scale from 0 (leading edge) to 1 (back of the lamellipodium) (Fig. 2e).

Both types of kinetics resulted in a linear decay of intensity similar to those from experimental data, producing similar intensity profiles. However, concentration curves based on contrast were different for the two types of depolymerization

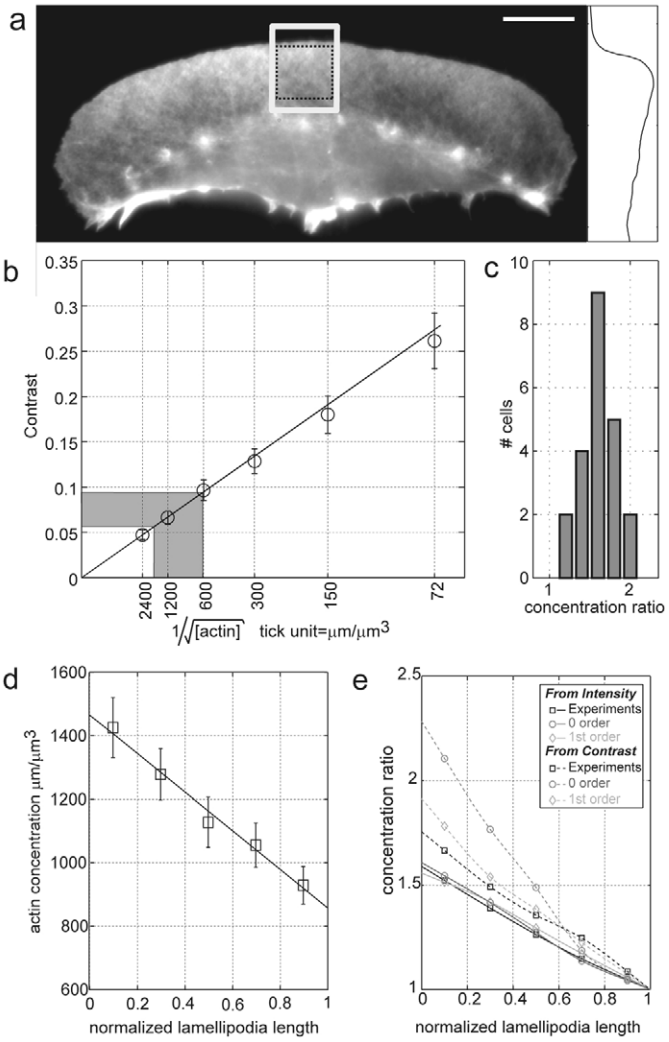

Fig. 2. Actin concentration analysis. (a) Distribution of F-actin in keratocyte visualized with Rhodamine-phalloidin. Actin-concentration profile from front to back of a lamellipodium (boxed gray region) is plotted at the right panel. Black dashed box represents a typical (7×7 μm^2) field of interest. Bar, 10 μm. (b) Contrast of the simulated images (circles) is plotted versus the inverse square root of actin-polymer concentration. Error bars give ± s.d. Gray area shows the range of contrast measured in experimental images and the corresponding range of actin concentration. (c,d) Histogram of the intensity ratio between front and back of a lamellipodium using measurements based on phalloidin-staining intensity (c), showing the same decay as the concentration profile measured by experimental contrast (d). Error bars give ± s.d. (e) Comparison of relative concentration profiles measuredon the basis of intensity (solid lines), contrast (dashed lines), in experimental (squares) and simulated images with zero-order and first-order depolymerization kinetics (circles and diamonds, respectively).

kinetics. The concentration ratios between front and back were measured at ~2.3 and ~1.84 for zero and first order kinetics, respectively. The second value is close to the experimental ratios based on intensity or contrast (1.6 or 1.73, respectively). Thus, from front to back of the lamellipodium, the change in contrast with concentration is consistent with first order actin depolymerization kinetics.

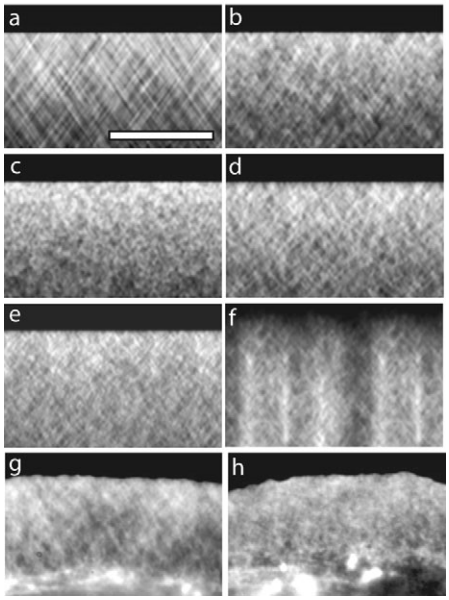

Fig. 3. Comparison of patterns of experimental and simulated fluorescence images of lamellipodia. (a-d) Dependence of the pattern on the mean filament length and orientation-disorder parameters in simulated fluorescence images. Low-disorder parameters (R=500 μm, $\delta\theta$=1°) and a mean filament length of (a) 4 μm, (b) 1 μm and (c) 0.3 μm and, (d) intermediate-disorder parameters (R=20 μm, $\delta\theta$=20°) and filament length of 4 μm. Simulated image with optimal parameters (L=1.3 μm, R=10 μm, $\delta\theta$=20°) built from stochastic processes (e) compared with the deterministic process of Arp2/3 activation (f). (g,h) Experimental image of equivalent sizes; (g) untreated cell and (h) cell treated with 0.1 μM cytochalasin D. Bar, 10 μm.

Analysis of filament length and orientation

Contrary to contrast, the pattern of the simulated images was strongly dependent on mean filament length $\Delta\theta$ and R_0 but little on the concentration. We simulated actin networks with a mean filament length of 4 μm to 300 nm (Fig. 3a,c). The patterns showed linear features oriented at approximately ±35° with respect to the normal to the leading edge, with the length of the features depending on mean filament length. For the shortest filaments, a linear pattern in the network was hardly noticeable (Fig. 3c), and the images were similar to speckle images. Longer filaments resulted in the criss-cross pattern of diagonal linear features. At very low parameter values the of filament curvature and branching angle fluctuation the criss-cross pattern in simulated images appeared more regular and clearer than in experimental images (Fig. 3a,g). Fluctuation of branching angle and filament curvature reduced the regularity of the pattern, and the length of the diagonal features (Fig. 3a,d). At intermediate parameters values, simulation yielded patterns similar to the experimental images of keratocyte lamellipodia (Fig. 3e). Keratocytes treated with low concentration of cytochalasin D (Fig. 3h) exhibited lamellipodia with a speckled pattern similar to simulations with short filaments (Fig. 3c), a results consistent with the capping activity of cytochalasin D that reduced mean filament length.

We tested whether probabilistic branching and capping were essential to generate patterns similar to experimental images.

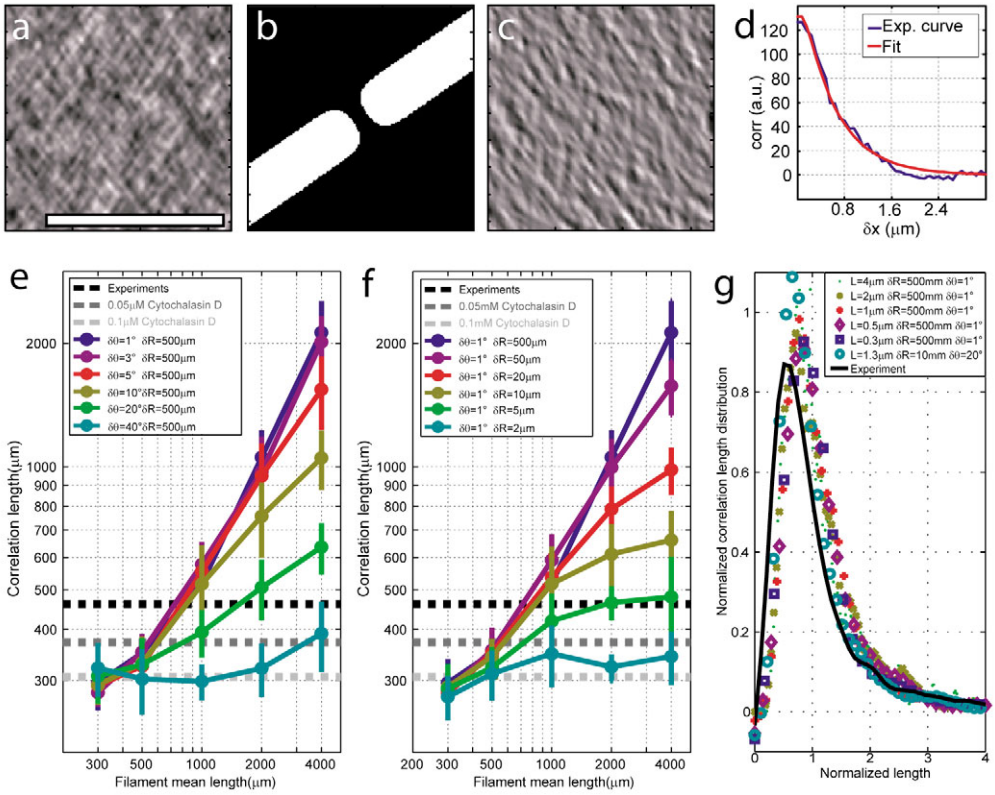

Fig. 4. Correlation-length analysis. (a-c) Square regions of the images (a) were filtered through Fourier mask (b) to highlight features along one orientation (c). Correlation curves measured along this direction (d, blue) were fitted (d, red) with theoretical correlation function to obtain the correlation length. (e,f) Mean correlation length measured in simulated images (solid lines) varies, depending on the mean filament length, (e) branching angle fluctuation and (f) curvature radius. Curves were compared with experimental correlation length measured in untreated cells (dashed black lines) and in cells treated with cytochalasin D at 0.05 μM (dark gray line) and 0.1 μM (light gray line). (g) Comparison of normalized correlation-length distributions from simulated images with different sets of parameters (colored symbols) to experimental images (black curve).

Instead of random branching at every time step we imposed a deterministic distribution of branching activity along the leading edge, the images displayed bright and dark bands perpendicular to the leading edge (Fig. 3f). These bands were not present in the experimental images, indicating that branching activity fluctuated randomly rather than being distributed deterministically along the edge. For objective comparison of the experimental and simulated images, it was necessary to obtain a quantitative measure of the length and orientation of the apparent diagonal features. We therefore developed a tool based on correlation length (see Materials and Methods). Correlation length provides information on the similarity of features depending on the distance along a line: the longer the features the slower the decay of the correlation curve. First, we measured correlation length in simulated images along the ±35° directions and observed that it depended strongly on filament length and orientation-disorder parameters (Fig. 4e,f). For very low orientation-disorder parameters, the correlation length was almost proportional to the filament length. For very short filaments, correlation length tended to plateau at ~200 nm, independently of the orientation-disorder parameters. This was consistent with the resolution limits of the light microscope (see below, Fig. 5b). Similar correlation lengths were measured on images of random speckle patterns convoluted with the microscope diffraction spot (not shown). For longer filaments, increasing any of the orientation-disorder parameters resulted in a decrease of the correlation length.

To measure the correlation length of experimental images, we first removed the overall gradient of intensity from front to back of the lamellipodium that was due to actin depolymerization. This gradient was removed by dividing the intensity of each image pixel by the mean intensity of the line parallel to the leading edge where this pixel belonged. In the resulting image, the mean intensity of the lines parallel to the leading edge did not decrease with the distance from the edge. Subsequently, correlation length was determined using the same procedure as for simulated images. Each image provided several hundred correlation-length measurements, thus allowing us to obtain the distribution of correlation length (Fig. 4g). To compare the distribution profiles in simulated and experimental images, we normalized the distribution curves by both the curve area and the mean correlation length. All distribution curves from simulated images were identical and very similar to the distribution curves from experimental images (Fig. 4g). Since the correlation length is related to the filament length, this result supports our assumptions about filament length distribution.

In principle, if the size of the region of interest is small with respect to the correlation length, the measured distribution of

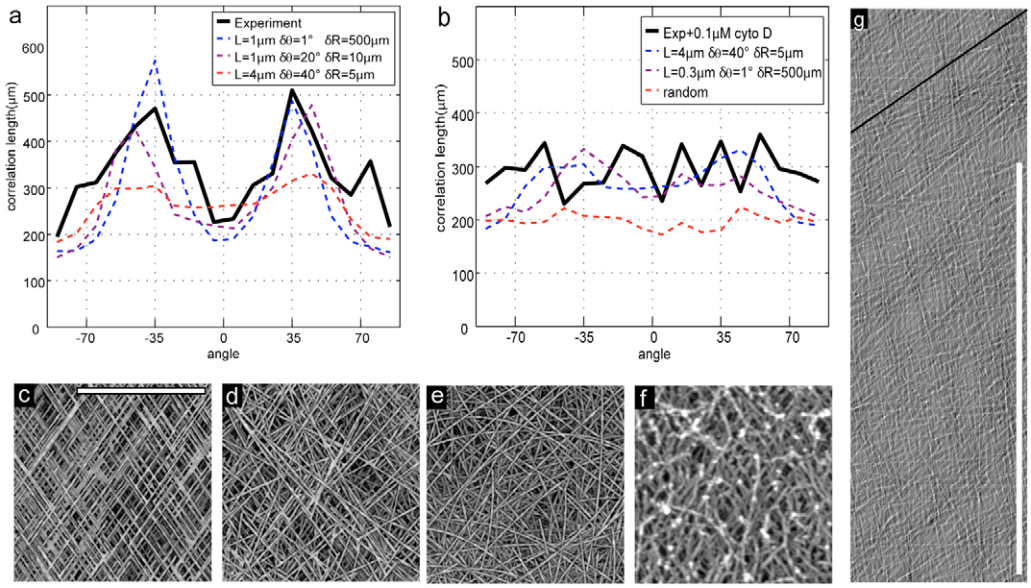

Fig. 5. Analysis of filament orientation and fit of simulated optical and EM images to the experimental images. (a) Angular distribution of correlation length in experimental (solid curves) and simulated (dashed curves) images. (b) Comparison of correlation-length distribution in cells treated with 0.1 μM of cytochalasin D with simulated distributions with short (or long) filaments and high (or low) orientational disorder parameters. The angle was measured with respect to the normal to the leading edge. (c-e) Simulated platinum replica images (c-e) created on the basis of the same simulations as in (a) and compared with a real platinum replica image (f) (provided T. M. Svitkina and G. G. Borisy). (g) A simulated negative staining EM image with the same parameters. Diagonal black line is parallel to the leading edge. Bar, 1 μm.

the correlation length may be biased towards short filaments. However, both the similarity between the simulated distributions (irrespective of the correlation length; Fig. 4g) and the proportionality of correlation length to the mean filament length for low disorder-parameter values (Fig. 4e,f) indicated that – for a mean filament length of up to 4 μm – the size of the region of interest did not induce a bias in the measurement of the correlation length.

Correlation length was estimated to be ~470 nm for experimental images, which corresponded to ~800-nm-long filaments in the case of low orientation disorder. For cells treated with cytochalasin D at 0.05 μM and 0.1 μM the correlation length was lower, and inversely correlated with the drug concentration, consistent with a reduction in mean filament length. We concluded that a mean filament should be at least 800 nm long in untreated cells and significantly shorter in the cells treated with cytochalasin D. However, these measurements did not allow us to distinguish between 800-nm-long filaments with a high degree of orientation order and longer orientation-disordered filaments.

Orientation disorder in the actin network produces filaments that are not oriented along ±35° directions. To investigate the contribution of orientation disorder in more detail, we obtained the angular distribution of correlation length (Fig. 5a) for both experimental and simulated images. The distributions presented two peaks at approximately +35° and –35°, with the peak heights consistent with previous measurements of correlation length for the two preferred directions (Fig. 4e,f). We observed that the peaks were sharper for low orientation-disorder parameters and wider for higher parameter values. The experimental curve presented an intermediate behavior and comparison with simulation data provided an estimated filament length of ~1.3 μm, a curvature radius of 10 μm and a branching angle variation of 20°.

Cells treated with 0.1 μM of cytochalasin D presented an almost flat distribution of correlation length (Fig. 5b). This distribution was similar to those simulated with short filaments and/or high disorder parameters. In both these cases, no preferential angles were seen. However, these distributions were different to those obtained from random dots convoluted with the diffraction spot, suggesting that lamellipodia of cells treated with cytochalasin D were not completely disorganized. Our analysis did not distinguish whether the predominant effect of cytochalasin D was filament shortening or scattering of angular distribution.

We also compared simulated EM images to experimental images. Simulated images clearly displayed scattering of filament orientation depending on the orientation-disorder parameters (Fig. 5c,e). Comparison with experimental images (Fig. 5f, image provided by T. M. Svitkina and G. G. Borisy University of Pennsylvania, Philadelphia, PA and MBL, Woods Hole, MA) suggested that intermediate orientation-disorder parameters (Fig. 5d) provided the best fit between experiments and simulations. Thus, the search for optimal parameters of filament length and orientation disorder around two preferred directions, in both optical and EM images, converges to an estimate of ~1.3 μm of filament length and ~20° of orientation-disorder parameters for angle fluctuation and ~10 μm for curvature radius.

Discussion

In this study, we evaluated structural parameters of the lamellipodium, such as actin filament density, length, angular distribution and curvature, by creating simulated images and

comparing them to experimental ones. To simulate the images, we first created the virtual actin network using the algorithm based on the dendritic branching model of the network assembly (Carlier et al., 2003; Pollard et al., 2000; Pollard and Borisy, 2003). In these simulations, the network growth was assumed to be a stochastic process, that is, branching and capping reactions were distributed randomly along the leading edge and the filament orientation fluctuated around two approximately diagonal directions. Then, the virtual network was converted into 'optical' images using the point-spread function of optical microscope, and into 'EM' images using two different custom algorithms for platinum replica and negatively contrasted images. We systematically studied the effect of simulation parameters on the image properties and, for a set of parameters, obtained images exhibiting a high degree of similarity to experimental images both visually and by objective criteria based on image intensity, contrast, correlation length and angular distribution.

The first implication of the similarity between experimental and simulated images is that the dendritic nucleation mechanism, with random branching and capping reactions, is sufficient to account for the image pattern observed in lamellipodia. More importantly, our image analysis not only provides support to the dendritic nucleation model, but also allows to estimate the important network parameters. Conclusions about the network parameters were made at two levels. First, by comparing simulated images with known filament properties to experimental images, we can evaluate structural network properties, such as length and orientation distribution of filaments. Second, in a more indirect model-dependent way, we also infer some parameters of network dynamics, such as the capping rate and the kinetic mechanism of the filament disassembly. In the first part of the study, we analyzed the variation in intensity of fluorescence images and demonstrated that random fluctuations in branching and capping are sufficient to create the variation of actin density that is observed experimentally in keratocyte lamellipodia. We established that it is independent on the initial concentration and distribution of actin network, and only depends on capping and branching rates (data not shown). We used the contrast of fluorescence images as a means to measure the variation in actin density and related these measurements to the filamentous actin concentration in the lamellipodia. Thus, measuring the contrast of optical images provided a novel approach to measure filamentous actin concentration. Our results were consistent with previous estimations of both the mean actin concentration (Abraham et al., 1999) and the concentration decay from the front to the back of the lamellipodium (Small et al., 1995; Svitkina and Borisy, 1999). If the actin concentration differed from the value predicted by our model for a given image contrast, it would suggest that actin density variation in the lamellipodium is not random. In particular, bundling of actin filaments with proteins like fascin (Svitkina et al., 2003) or fimbrin (Bartles, 2000; Small et al., 2002) would be expected to result in a contrast higher than predicted by the simulations. Localized protection of filament tips from capping could also create variation in actin concentration above the level predicted for a random process. Bundling and/or protection from capping may give rise to microspikes and filopodia. In contrast to many other cell types, epidermal fish keratocytes do not display morphologically recognizable microspikes within their lamellipodia, but exhibit an apparent loose grouping of filaments into criss-cross linear pattern (Verkhovsky et al., 2003). It cannot be completely excluded that bundling proteins with a long crosslinking distance and/or localized protection from capping contribute to the formation of this pattern. However, our present study strongly suggests that these processes are not significant in the keratocyte lamellipodia, because actin density variation is fully accounted for by the random reactions nucleation and capping. The fast motion of keratocytes suggests that microspike-like bundles are not an intrinsic part of the effective motile machinery. We expected that, by refining our model to include filament bundling processes, we were able to mimic lamellipodia containing microspikes as well. Stochastic processes were essential to reproduce pattern of the experimental images. In particular, deterministic distribution of Arp2/3 activation along the leading edge resulted in dark and bright band perpendicular to the leading edge which was not observed experimentally (Fig. 3f).

Simulations provided both qualitative (visual comparison of the fluorescence and EM images) and quantitative (correlation length and its angular distribution) approaches to estimate mean filament length and orientation distribution. These estimations converged to a single set of parameters providing the best fit between simulated and experimental images. In particular, mean filament length was estimated at approximately 1.3 μm. Previous estimations of filament length ranged from a few hundred nanometers based on capping kinetics in a cell lysate (Cano et al., 1991) to several micrometers based on examination of negatively contrasted EM images (Small et al., 1995). Our estimation is in the middle of this range. It was argued that, in order to push the membrane effectively, the filament needs to be sufficiently rigid and thus cannot exceed few hundreds of nanometers in length (Mogilner and Oster, 2003). However, in the lamellipodium, the filament network is very dense in the vicinity of the membrane and the crosslinking and crowding of the network may stabilize and reinforce longer filaments, reducing their free effective length and enabling them to exert pressure on the membrane in a synergetic manner. This effect cannot be estimated by analysing optical images because stabilization of the filaments in the network is not expected to change the distribution of fluorescence intensity.

Our simulations are also consistent with the observations of very long filaments (several micrometers) in negatively stained EM specimens (Small et al., 1995). With a mean filament length of 1.3 μm, simulated negatively stained EM images were comparable to experimental images (e.g. Small et al., 1995, fig. 3 within compare with Fig. 5g this article). To estimate the contribution of long filaments to the image, we also created images where only filaments longer than 2.2 μm were retained (supplementary material Fig. S1, note that this length is larger than the size of the displayed part of the image). Based on the distribution of filament length, filaments longer than 2.2 μm represent $(1+l/\lambda)e^{-l/\lambda}$=50% of the mass of the actin network. This might explain the impression of the abundance of the long filaments in the population.

The angular distribution of correlation length exhibited two peaks around ±35°, suggesting preferential orientation of filaments along these two directions. We previously measured the orientation of features in phase-contrast, fluorescence and

platinum-replica images (Verkhovsky et al., 2003) using a different method, i.e. modified Radon transform. Here, we confirmed our previous result for fluorescence images, and our new approach developed has an advantage over Radon transform because it provides the simultaneous estimation of filament orientation and length.

Knowing the mean filament length and velocity of keratocyte crawling (approximately 15 μm/minute), we estimated the capping rate constant to be:

$$k_c = \frac{v}{\lambda \cos(35°)} = 0.23\ s^{-1}. \quad (3)$$

This value is in accordance with a previous estimation (Carlsson, 2003). Note that the capping rate estimated in vitro may be different from that of lamellipodia, due to reduction of the diffusion rate in a dense network and/or factors protecting filaments from capping. Note also that the same capping rate would produce shorter filaments if the cell velocity is slower than that of a keratocyte. Thus, slower moving cells may have shorter filaments. One important limitation of our estimation of the capping rate is its dependence on the specifics of the network-growth model. In particular, it is based on the assumption that the length of the filament does not change after the capping event. In our model, we assumed that when the filament is affected by depolymerization, it disappears instantly in a single event, which is consistent with the cooperative nature of ADF/cofilin activity (Pollard et al., 2000). If, however, the depolymerization reduces filament length gradually rather than eliminating filaments as a whole, the capping-rate constant may be overestimated based on the observed filament length. To evaluate the margin of error, we assume that all the filaments are depolymerized gradually and uniformly. Then, to reduce the actin density at the rear edge of the lamellipodium by a factor of 1.6, the length of each filament should be reduced by the same factor. Thus the filaments, immediately after capping, might be 1.5 times longer than at the back of the lamellipodium and the evaluation of the capping rate constant based on the filament length might, at worst, lead to an overestimate by the factor 1.5.

To investigate the specifics of the depolymerization kinetics, we analyzed the dependence of the image contrast and density on the distance from the leading edge. The introduction of depolymerization in simulations demonstrated a good fit between experiments and a simulated first order (with respect to actin filament concentration) depolymerization kinetics. This is consistent with the concentration of actin-bound ADF/cofilin being proportional to the concentration of actin filaments. By contrast, a zero-order process would suggest a homogeneous concentration of cofilin. Experiments showed similar decay of both actin and cofilin concentration profiles (Svitkina et al., 1997) providing additional support for the hypothesis of a first-order process for depolymerization. We did not consider filament severing properties of ADF/cofilin (Bamburg, 1999; Carlier et al., 1997; Ressad et al., 1998). Introduction of severing effects in our simulations would change the depolymerization rate, mean filament length and the capping rate. It would also alter the distribution of filament length, acting preferentially on the long filaments. If we consider the correlation length in the images as a measure of filament length, the close similarity between simulated and experimental distributions of correlation length would suggest that the effect of severing in lamellipodia is insignificant.

The approach proposed in this paper provides a novel way to study the structure and dynamics of lamellipodia. Modeling a limited number of reactions and taking advantage of the steady-state character of keratocyte locomotion to simplify our model, we were able to recreate the actin pattern observed in real lamellipodia. Patterns similar to experiments on a length range of several times the mean filament length were created on the basis of local stochastic rules. Additional components were introduced into the simulation to refine the model and make it applicable to a wider range of cell behavior. For example, introduction of filament bundling by fascin reproduced the image patterns characteristic of the lamellipodia with microspikes and filopodia. Our approach can also be applied to correlate actin network properties with motile behavior in different types of cell and elucidate the structural basis of persistent motility of cells (such as keratocytes) versus less persistent behavior of cells (such as leucocytes and cells from *Dictyostelium discoideum*). However, this would require adapting individual filament dynamics for each cell type. Image simulation provides an original method to test the accuracy of the model and allows evaluation of the model parameters. Even in its present simple form our in silico lamellipodia provided insight into some of the elusive features of actin networks, such as distribution of filament length and orientation.

Materials and Methods

Cell culture, treatment and staining

Black tetra (*Gymnocorymbus ternetzi*) keratocytes were cultured in DMEM supplemented with 10% fetal bovine serum and antibiotics as described (Verkhovsky et al., 2003). For experiments with cytochalasin D (Sigma), the cells were incubated in medium with 0.05 to 0.1 μM of cytochalasin D for 20 minutes before fixation. To visualize F-actin distribution, cells were fixed with glutaraldehyde, permeabilized with Triton X-100 and then stained with Rhodamine-phalloidin as described (Verkhovsky et al., 2003). By fixing the cells before permeabilization, we minimized the risk of loosing actin filaments from the cell during permeabilization and staining (Small et al., 1995). This fixation and staining procedure was previously employed to preserve the full F-actin contents of lamellipodia (Svitkina et al., 1997).

Microscopy

Optical microscopy was performed with the Nikon Eclipse TE300 inverted microscope with CFI Plan 100×/1.25 phase objective. Images were acquired with MicroMAX-1300PB cooled CCD camera (Roper Scientific, Trenton, NJ) controlled by Metamorph software (Universal Imaging, West Chester, PA).

Simulation of images

To simulate fluorescence microscopy images, we considered the properties of our microscope. The focus depth of the microscope is greater than the thickness of the lamellipodia; consequently, we considered all the filaments to be in focus and summed the fluorescence of all superimposed filaments (Fig. 1a,b). The area, magnification and resolution and of simulated images had to be set equal to the experimental images. Our model considers the assembly of actin network, but not the subsequent reorientation or movement of the filaments. Therefore, the simulated images are comparable with the main part of the lamellipodium, but not with the back of the lamellipodium where the filaments are presumably reoriented by myosin motors to form a large bundle (Svitkina et al., 1997). We also did not consider the vicinity of the leading edge (~0.5 μm) to avoid possible edge effects such as variation in lamellipodium thickness or possible loss of short filaments during fixation. Experimental images were thus cropped to approximately 7×7 μm^2 with the top boundary parallel to the leading edge and ~0.5 μm away from the leading edge (see Fig. 2a). Size of simulated images was determined by the interval length of initial actin-seed distribution and the number of iterations of network growth. Typically, simulated images were initially 24 μm wide (parallel to the edge) and 16 μm long (normal to the edge) and subsequently cropped to 7×7 μm^2.

The magnification of our acquisition system was 80 nm per pixel. To simulate optical images, the resolution of our simulation of network growth (4 nm) had to be reduced to the resolution level of the optical microscopy. The resolution of our

microscope has been estimated to be ~0.61×λ/NA (Born and Wolf, 1999). We confirmed this estimate by analyzing the distribution of light emitted by a microtubule, which may be considered as an infinitely thin line because its width is much smaller than the resolution limit. The diffraction patterns obtained theoretically and experimentally were identical (data not shown). We convoluted the results of the simulations with the diffraction spot of our microscope to obtain a resolution equivalent to experimental images (Fig. 1c).

To compare the simulated and real actin networks at a higher resolution level, we created images similar to either platinum replicas or negatively stained EM images. In the platinum-replica method, metal is sprayed on the surface of the sample, which preferentially enhances the top layer of the actin meshwork. Using the 3D position of the filaments, we created an image for each filament lineage with a unique and constant height. Next, we superimposed the different layers (the highest ones – being brighter – hiding the layers underneath). In the negative-staining EM method, the contrasting agent stains all filaments but the total intensity is fairly uniform irrespective of the filament concentration, unlike results obtained with fluorescence microscopy. We applied texture to both simulated replica and negatively stained images to create a more realistic pattern.

Measuring the correlation length

To measure the correlation length, we first obtained the correlation curves. The correlation curve of the intensity function $I(x)$ was defined as the mean of the products of the intensity of each pair of pixels which are δx pixel apart from each other after subtraction of the mean value of $I(x)$:

$$corr\,(\delta x) = \frac{1}{N_x} \sum_{x=1}^{N_x(\delta x)} [I(x)-\bar{I}] \cdot [I(x+\delta x)-\bar{I}]. \quad (4)$$

This function is equal to the variance for $\delta x=0$. If the intensity values are independent, the correlation curve approaches 0.

To analyze images, we measured correlation curves along specific directions, e.g. the preferred directions of filament growth, which are approximately ±35° to the direction of protrusion. To reduce contribution from features that were not oriented along the chosen direction and from features that were significantly larger than the lines in the characteristic criss-cross pattern visible in the optical images of the lamellipodia (Verkhovsky et al., 2003), we defined a mask in Fourier space and filtered images with this mask (Fig. 4a,c).

Next, we extracted the correlation length from the correlation curves. Correlation length is expected to be related to the filament length. Indeed, the fluorescence intensities of the two pixels located at a distance from each other are correlated if the filaments going through one pixel also reach the other pixel. In our model (see below, Model of network growth), the filament length is distributed according to a Poissonian law, defined by mean filament length. Thus, the correlation is expected to decay exponentially with the distance along the filament direction. For short distances, the diffraction in the optical microscope also contributes to the correlation. For this reason, the theoretical correlation function was defined as an exponential curve convoluted with a Gaussian curve, defined by the diffraction-spot size (see above, Simulation of images):

$$fit(\delta x,\lambda_c) = e^{-\delta x/\lambda_c} \times \frac{1}{\sigma\sqrt{\pi}}\, e^{-\delta x^2/\sigma^2}, \quad (5)$$

where δx is the distance along the selected direction and λ_c is the correlation length. We used this function to fit the correlation curves obtained from images (Fig. 4d) and then to measure the correlation length.

Model of network growth

Simulation of the network growth was performed using MatLab software (Mathworks). The algorithm was based on the dendritic nucleation and the array treadmilling model of the lamellipodial actin dynamics (Pollard et al., 2000). According to this model, the actin network is produced by successive reactions of branching, elongation and capping of filaments close to the leading edge of the cell. Subsequently, disassembly removes filaments from the network and provides subunits for continuous growth. We simulated images of the actin network – taking into account the reactions of branching, elongation and capping – to reproduce the variation of actin density and image contrast with distance from the edge. We also considered disassembly. We have previously demonstrated that the characteristic optical criss-cross pattern of the actin network becomes apparent at the very leading edge of the cell (Verkhovsky et al., 2003), whereas the disassembly of the actin network has been reported to occur at a distance from the edge (Svitkina and Borisy, 1999). Therefore, the disassembly reaction is probably not important for the formation of the image pattern and has only been considered in the analysis of actin concentration decay from the front to the back of lamellipodia.

We adopted several simplifying assumptions about the geometry of the simulated network based on the shape of keratocyte lamellipodia. The lamellipodium of a keratocyte is flat, wide and thin in vertical dimension. Its leading edge is almost straight at the central part and curved at the lateral sides; it advances smoothly at a nearly constant velocity. We focused on modeling the central part of the lamellipodium and, consequently, considered flat lamellipodium with a straight leading edge advancing at constant speed. The straightness of the leading edge allowed us to use periodic boundary conditions to solve the lamellipodium sides. To prevent filaments from growing faster than the leading edge, we let elongation, capping and nucleation occur at the barbed-end only when there was a distance between the filament tip and the leading edge. This condition was not intended to reproduce realistically the mechanism of interaction between the filaments and the membrane: in reality, growing filaments push the edge, rather than the advancing edge letting filaments grow. Nevertheless, the above condition synchronized the growth of all filaments with the advance of the leading edge. Thus, the spatial relationship between growing filament tips and the edge was reproduced accurately in our model. The filaments were constrained to grow in a plane parallel to the substrate. One can argue that, for other orientations, filaments reach quickly the apical or basal membrane and then either stop to elongate or bend to become parallel to the substrate. To simulate platinum replica images, we assigned a vertical position for each filament at the beginning of the simulation. Daughter filaments then inherited their vertical positions from mother filaments. The position of each filament was fixed in space and did not change during the subsequent network growth. This condition is consistent with the fact that actin filaments are nearly stationary with respect to the substrate in the front part of the keratocyte lamellipodium. Retrograde actin flow, which was recently detected in keratocytes (Vallotton et al., 2005), is slow with respect to the cell advance and nearly uniform in velocity in the central part of the lamellipodium, so it is not likely to induce significant displacement of the filaments with respect to each other. Another possible reason for filament displacement could be the network contraction powered by myosin II, which was proposed to bend and align filament at the transition zone between lamellipodium and cell body (Svitkina et al., 1997). However, the contraction is localized to the rear of the lamellipodium (Svitkina et al., 1997; Verkhovsky et al., 1999), which is excluded from the analyzed regions of interest of experimental images. The effect of contraction could, therefore, be neglected for the front and central part of the lamellipodium.

Capping and nucleation reactions have opposite effects on the total number of growing filament ends. This number is expected to remain constant during steady state network growth. We defined the capping and nucleation rate parameters in the following way: the capping probability per time unit and per filament (p_c) and the number of new branches created per time unit and length unit along the leading edge (N_b). Thus, capping and branching were defined as reactions of different order with respect to the free barbed-end concentration (first and zero order, respectively). This assumption is in agreement with experimental data: first-order rate for capping was measured in in-vitro assays (Mullins and Pollard, 1999; Xu et al., 1999), whereas the WASP/Scar activation of branching was suggested to be the limiting factor of network growth (Pollard et al., 2000), which is consistent with a zero-order process. With thus defined branching and capping rate constants, the free barbed-end concentration reaches a steady state value $[E_f]$ such that $N_b=p_c\times[E_f]$ irrespective of the conditions at the start of simulation (data not shown). For the first order capping reaction, the filament length distribution D_λ was defined as: $D_\lambda(i)=p_c(1-p_c)_i\cong p_c\times e^{-l\cdot p_c}$ and, therefore, $\langle\lambda\rangle=1/p_c$, where $\langle\lambda\rangle$ is the mean filament length.

The simulation of network growth consisted of the dynamics of each individual filament. At each time step, we tested whether the barbed-end of each filament was capped; if not, the filament continued to polymerize (Fig. 1a). Activation of the branching factor occurred randomly along the leading edge. Next, we assigned the formation of the new daughter filament to the filament tip closest to the activation event (Fig. 1a). Different authors have reached different conclusions regarding the exact site of the new branch formation, either at the tip of the filament (Pantaloni et al., 2000; Pantaloni et al., 2001) or at its side (Blanchoin et al., 2000; Higgs and Pollard, 2001). Despite this difference of opinions, it is widely accepted that, in protruding lamellipodia, branching is strongly favored in the zone very close to the leading edge. We imposed branching at the tip of the filament, but no significant difference was seen if the branching occurred at a random position in the range of two hundred nanometers from the tip (data not shown).

Orientation of the filaments was defined as being distributed according to a Gaussian law (with the width at half height $\Delta\theta$) around one of the two main orientations, either +35° or –35° with respect to the normal leading edge. Between these two orientations, we chose for each daughter filament the one yielding an angle between mother and daughter filament closest to 70°. In reality, the orientation of the daughter filament is established with respect to the mother filament, not with respect to the leading edge. However, overall filament orientation distribution preferentially displays two symmetric directions approximately diagonal to the leading edge (Small et al., 1995). It was proposed that this distribution resulted from the competitive selection of filament families having the best chance to proliferate at the leading edge (Maly and Borisy, 2001). We did not consider the dynamic process of filament orientation selection in our model, but we imposed that the final distribution of filaments reflected the result of this selection process. The Gaussian distribution around two preferential directions was chosen as the most natural possibility in the absence of the exact knowledge about the character of this distribution.

We also allowed filament bending. A homogeneous curvature radius was randomly assigned to each filament according to a decaying exponential distribution

scaled by R_0, the inverse of mean curvature. The curvature of the filaments in a lamellipodium probably results from mechanical constraints experienced by each filament during network growth. We imposed the distribution of curvature without considering the detailed bending forces acting on the filaments. The simplest model of fluctuation for a fiber curvature is, on the basis of elastic bending energy, expected to follow a scaled exponential distribution, based on elastic bending energy.

Since capping and branching were linked to each other in a steady-state equilibrium by free barbed-end concentration, we considered only one parameter for the two processes, i.e. mean filament length. Thus, the whole lamellipodium was defined by the mean filament length $\langle\lambda\rangle$, the mean actin polymer concentration $[A]$, the branching angle fluctuation $\Delta\theta$ and the curvature radius R_0. The last two parameters are referred to as orientation disorder in the lamellipodium.

In most simulations, we did not consider actin depolymerization. Depolymerization was only considered when we analyzed the variation of actin density and image contrast with the distance from the leading edge (see Results). We assumed that only those capped filaments were depolymerized whose barbed ends were further than 1 μm from the leading edge. This is consistent with the localization of ADF/cofilin in keratocyte lamellipodia and with the fact that the filaments containing ATP-actin are protected from its action (Svitkina and Borisy, 1999). Note that depolymerization in our model did not affect actin density at the leading edge. This density was determined by the balance of branching and capping, irrespective of depolymerization. An entire filament was depolymerized in a single event. This is consistent with the cooperative mechanism of the action of ADF/cofilin (De La Cruz, 2005; Pollard et al., 2000). We defined two alternative kinetics for depolymerization, a first-order and a zero-order kinetics. The first order process was defined by the probability for each filament to be disassembled and, thus, the total depolymerization rate was proportional to filament concentration. This is consistent with depolymerizing factors (ADF/cofilin) being in excess. For the zero-order process, a fixed number of capped filaments were removed at random from the lamellipodium per time step. This is consistent with the process being limited by a fixed concentration of the depolymerizing factor.

This study was supported by Swiss National Science Foundation grant 31-61589. We are grateful to Tatyana Svitkina, Oleg Chaga and Gary Borisy for critical discussions and platinum replica images of keratocyte lamellipodia, and to James Sillibourne for technical help.

References

Abraham, V. C., Krishnamurthi, V., Taylor, D. L. and Lanni, F. (1999). The actin-based nanomachine at the leading edge of migrating cells. *Biophys. J.* **77**, 1721-1732.

Anderson, K. I., Wang, Y. L. and Small, J. V. (1996). Coordination of protrusion and translocation of the keratocyte involves rolling of the cell body. *J. Cell Biol.* **134**, 1209-1218.

Bamburg, J. R. (1999). Proteins of the ADF/cofilin family: essential regulators of actin dynamics. *Annu. Rev. Cell Dev. Biol.* **15**, 185-230.

Bartles, J. R. (2000). Parallel actin bundles and their multiple actin-bundling proteins. *Curr. Opin. Cell Biol.* **12**, 72-78.

Bear, J. E., Rawls, J. F. and Saxe, C. L., 3rd (1998). SCAR, a WASP-related protein, isolated as a suppressor of receptor defects in late Dictyostelium development. *J. Cell Biol.* **142**, 1325-1335.

Bear, J. E., Svitkina, T. M., Krause, M., Schafer, D. A., Loureiro, J. J., Strasser, G. A., Maly, I. V., Chaga, O. Y., Cooper, J. A., Borisy, G. G. et al. (2002). Antagonism between Ena/VASP proteins and actin filament capping regulates fibroblast motility. *Cell* **109**, 509-521.

Blanchoin, L., Amann, K. J., Higgs, H. N., Marchand, J. B., Kaiser, D. A. and Pollard, T. D. (2000). Direct observation of dendritic actin filament networks nucleated by Arp2/3 complex and WASP/Scar proteins. *Nature* **404**, 1007-1011.

Born, M. and Wolf, E. (1999). Image formation in the microscope. In *Principles of Optics, Electromagnetic Theory of Propagation, Interference and Diffraction of Light* (7th edn), pp. 465-475. Cambridge: Cambridge University Press.

Cano, M. L., Lauffenburger, D. A. and Zigmond, S. H. (1991). Kinetic analysis of F-actin depolymerization in polymorphonuclear leukocyte lysates indicates that chemoattractant stimulation increases actin filament number without altering the filament length distribution. *J. Cell Biol.* **115**, 677-687.

Carlier, M. F., Laurent, V., Santolini, J., Melki, R., Didry, D., Xia, G. X., Hong, Y., Chua, N. H. and Pantaloni, D. (1997). Actin depolymerizing factor (ADF/cofilin) enhances the rate of filament turnover: implication in actin-based motility. *J. Cell Biol.* **136**, 1307-1322.

Carlier, M. F., Le Clainche, C., Wiesner, S. and Pantaloni, D. (2003). Actin-based motility: from molecules to movement. *BioEssays* **25**, 336-345.

Carlsson, A. E. (2003). Growth velocities of branched actin networks. *Biophys. J.* **84**, 2907-2918.

De La Cruz, E. M. (2005). Cofilin binding to muscle and non-muscle actin filaments: isoform-dependent cooperative interactions. *J. Mol. Biol.* **346**, 557-564.

Gupton, S. L., Anderson, K. L., Kole, T. P., Fischer, R. S., Ponti, A., Hitchcock-DeGregori, S. E., Danuser, G., Fowler, V. M., Wirtz, D., Hanein, D. et al. (2005). Cell migration without a lamellipodium: translation of actin dynamics into cell movement mediated by tropomyosin. *J. Cell Biol.* **168**, 619-631.

Higgs, H. N. and Pollard, T. D. (2001). Regulation of actin filament network formation through ARP2/3 complex: activation by a diverse array of proteins. *Annu. Rev. Biochem.* **70**, 649-676.

Maly, I. V. and Borisy, G. G. (2001). Self-organization of a propulsive actin network as an evolutionary process. *Proc. Natl. Acad. Sci. USA* **98**, 11324-11329.

Marcy, Y., Prost, J., Carlier, M. F. and Sykes, C. (2004). Forces generated during actin-based propulsion: a direct measurement by micromanipulation. *Proc. Natl. Acad. Sci. USA* **101**, 5992-5997.

Mogilner, A. and Oster, G. (1996). Cell motility driven by actin polymerization. *Biophys. J.* **71**, 3030-3045.

Mogilner, A. and Oster, G. (2003). Force generation by actin polymerization II: the elastic ratchet and tethered filaments. *Biophys. J.* **84**, 1591-1605.

Mullins, R. D. and Pollard, T. D. (1999). Rho-family GTPases require the Arp2/3 complex to stimulate actin polymerization in Acanthamoeba extracts. *Curr. Biol.* **9**, 405-415.

Mullins, R. D., Heuser, J. A. and Pollard, T. D. (1998). The interaction of Arp2/3 complex with actin: nucleation, high affinity pointed end capping, and formation of branching networks of filaments. *Proc. Natl. Acad. Sci. USA* **95**, 6181-6186.

Pantaloni, D., Boujemaa, R., Didry, D., Gounon, P. and Carlier, M. F. (2000). The Arp2/3 complex branches filament barbed ends: functional antagonism with capping proteins. *Nat. Cell Biol.* **2**, 385-391.

Pantaloni, D., Le Clainche, C. and Carlier, M. F. (2001). Mechanism of actin-based motility. *Science* **292**, 1502-1506.

Peskin, C. S., Odell, G. M. and Oster, G. F. (1993). Cellular motions and thermal fluctuations: the Brownian ratchet. *Biophys. J.* **65**, 316-324.

Pollard, T. D. and Borisy, G. G. (2003). Cellular motility driven by assembly and disassembly of actin filaments. *Cell* **112**, 453-465.

Pollard, T. D., Blanchoin, L. and Mullins, R. D. (2000). Molecular mechanisms controlling actin filament dynamics in nonmuscle cells. *Annu. Rev. Biophys. Biomol. Struct.* **29**, 545-576.

Resch, G. P., Goldie, K. N., Krebs, A., Hoenger, A. and Small, J. V. (2002). Visualisation of the actin cytoskeleton by cryo-electron microscopy. *J. Cell Sci.* **115**, 1877-1882.

Ressad, F., Didry, D., Xia, G. X., Hong, Y., Chua, N. H., Pantaloni, D. and Carlier, M. F. (1998). Kinetic analysis of the interaction of actin-depolymerizing factor (ADF)/cofilin with G- and F-actins. Comparison of plant and human ADFs and effect of phosphorylation. *J. Biol. Chem.* **273**, 20894-20902.

Small, J. V. (1995). Getting the actin filaments straight: nucleation-release or treadmilling? *Trends Cell Biol.* **5**, 52-55.

Small, J. V., Herzog, M. and Anderson, K. (1995). Actin filament organization in the fish keratocyte lamellipodium. *J. Cell Biol.* **129**, 1275-1286.

Small, J. V., Stradal, T., Vignal, E. and Rottner, K. (2002). The lamellipodium: where motility begins. *Trends Cell Biol.* **12**, 112-120.

Svitkina, T. M. and Borisy, G. G. (1999). Arp2/3 complex and actin depolymerizing factor/cofilin in dendritic organization and treadmilling of actin filament array in lamellipodia. *J. Cell Biol.* **145**, 1009-1026.

Svitkina, T. M., Verkhovsky, A. B., McQuade, K. M. and Borisy, G. G. (1997). Analysis of the actin-myosin II system in fish epidermal keratocytes: mechanism of cell body translocation. *J. Cell Biol.* **139**, 397-415.

Svitkina, T. M., Bulanova, E. A., Chaga, O. Y., Vignjevic, D. M., Kojima, S., Vasiliev, J. M. and Borisy, G. G. (2003). Mechanism of filopodia initiation by reorganization of a dendritic network. *J. Cell Biol.* **160**, 409-421.

Vallotton, P., Danuser, G., Bohnet, S., Meister, J. J. and Verkhovsky, A. B. (2005). Tracking retrograde flow in keratocytes: news from the front. *Mol. Biol. Cell* **16**, 1223-1231.

Verkhovsky, A. B., Svitkina, T. M. and Borisy, G. G. (1999). Self-polarization and directional motility of cytoplasm. *Curr. Biol.* **9**, 11-20.

Verkhovsky, A. B., Chaga, O. Y., Schaub, S., Svitkina, T. M., Meister, J. J. and Borisy, G. G. (2003). Orientational order of the lamellipodial actin network as demonstrated in living motile cells. *Mol. Biol. Cell* **14**, 4667-4675.

Xu, J., Casella, J. F. and Pollard, T. D. (1999). Effect of capping protein, CapZ, on the length of actin filaments and mechanical properties of actin filament networks. *Cell Motil. Cytoskeleton* **42**, 73-81.